FAST TRACK COMMUNICATION • OPEN ACCESS

Enhanced synchronization due to intermittent noise

New Journal of Physics
The open access journal at the forefront of physics

Deutsche Physikalische Gesellschaft DPG
IOP Institute of Physics

Published in partnership with: Deutsche Physikalische Gesellschaft and the Institute of Physics

OPEN ACCESS

RECEIVED
19 August 2021

REVISED
7 November 2021

ACCEPTED FOR PUBLICATION
10 November 2021

PUBLISHED
23 November 2021

FAST TRACK COMMUNICATION

Enhanced synchronization due to intermittent noise

Emilda Shajan[1], M Paul Asir[1], Shiva Dixit[1,2], Jürgen Kurths[3,4,5] and Manish Dev Shrimali[1,*]

[1] Department of Physics, Central University of Rajasthan, Ajmer 305 817 India
[2] Department of Physics, Indian Institute of Technology Bombay, Powai, Mumbai 400 076, India
[3] Institute of Physics, Humboldt-University, Berlin 10099, Germany
[4] Potsdam Institute for Climate Impact Research, Potsdam 14473, Germany
[5] Lobachevsky University of Nizhny Novgorod, Nizhnij Novgorod 603950, Russia
[*] Author to whom any correspondence should be addressed.

E-mail: shrimali@curaj.ac.in

Keywords: synchronization, noise, chaotic system

Abstract

We propose a novel scheme to regulate noise infusion into the chaotic trajectories of uncoupled complex systems to achieve complete synchronization. So far the noise-induced synchronization utilize the uncontrolled noise that can be applied in the entire state space. Here, we consider the controlled (intermittent) noise which is infused in the restricted state space to realize enhanced synchronization. We find that the intermittent noise, which is applied only to a fraction of the state space, restricts the trajectories to evolve within the *contraction region* for a longer period of time. The basin stability of the synchronized states (SS) is found to be significantly enhanced compared to uncontrolled noise. Additionally, we uncover that the SS prevail for an extended range of noise intensity. We elucidate the results numerically in the Lorenz chaotic system, the Pikovski–Rabinovich circuit model and the Hindmarsh–Rose neuron model.

1. Introduction

An adjustment of rhythms among coupled oscillating units can be broadly emphasized as the phenomenon of synchronization [1]. It has a wider significance across various disciplines, such as physics, chemistry, biology, engineering and sociology. In the past couple of decades, the phenomenon of synchronization in chaotic systems and relevant theories have attracted a lot of attention [2, 3]. Numerous synchronization schemes were proposed, such as active control [4], nonlinear control [5, 6], adaptive control [7] and back-stepping design [8] to attain complete synchronization. Regardless of coupling schemes or control, one can also achieve synchronized states (SS) by driving the oscillators with a common noise or a periodic forcing [9, 10]. In the pioneering work of noise-induced harmony, a map representing the Belousov–Zhabotinsky (BZ) chemical reaction was found to transit from chaotic to ordered behavior with the addition of noise [11]. Inspired from these theoretical results, experimental observation of noise-induced synchronization (NIS) have been attested in the BZ reaction [12], chaotic Chua circuit [13], biological uncoupled sensory neurons [14], etc. Analytical and numerical results confirming the NIS in chaotic maps and the Lorenz model have been presented [15]. Also, synchronization properties of uncoupled limit cycle oscillators driven by common and individual noises speculates that in addition to synchronization one may suspect clustering or more generally coherence in such systems [16]. Further, noise-induced synchrony has been found in globally coupled phase oscillators with weaker interaction strength [17] and recently in complex networks with diffusive interaction [18]. This effect is likely to occur due to the convergence of chaotic trajectories into the laminar region for an infinitely long time than in the absence of noise. Precisely, it was shown that a common Gaussian noise tames the trajectories into the stable manifold of the saddle fixed points which in turn attribute to negative transverse Lyapunov exponents. Common noise has a huge relevance in biology and ecology as well. Synchronous environmental shocks have been correlated with noise to assimilate the rhythmic population dynamics of sheep in two islands [19]. Also, the reliability of repetitive spiking of neocortical neurons due to underlying noisy

mechanisms is an epitome of NIS in neurology [20]. The latest experimental results on NIS reveals that the minimum noise strength required to induce frequency locking raises with the amplitude of the oscillators but decreases as the number of oscillators in the network increases [21]. Also, rhythmic macroscopic activity of excitable neurons has been found under the influence of common noise with application to deep brain simulation of Parkinson's disease [22]. The uncoupled excitable Fitzhugh–Nagumo neurons were also found to display synchronized activity under the influence of common white and colored noise [23]. In the recent past, the stochastic bits generated by superparamagnetic junctions have been found to be phase-locked by infusing colored noise [24]. Moreover, the recent advances in synchronization research reveal the occurrence of explosive/discontinuous transition to SS in an oscillator network [25–27]. A few recent reviews account the phenomenon in detail [28, 29]. Interestingly, double explosive transitions have been identified at the emergence of cooperation in evolutionary games [30]. In addition, the population of cooperative and competitive oscillators was found to exhibit continuous and explosive transitions by adjusting the balance between oscillator types [31]. A generalized model for discontinuous transition and time-dependent rhythmic states were introduced by altering the Kuramoto model with positive feedback [32]. The synchronization problem of stochastic delayed multilayer networks has also been dealt with specific control strategies [33]. Further, few state of art investigations on synchronization enhances our understanding of the phenomena in diversified networks [34–42].

Analogous to NIS, weak interaction can also lead to synchronization [1]. A dynamic interaction that is active only in a subset of the state space constitutes a paramount significance in synchronizing chaotic systems [43, 44]. The mechanism of transient uncoupling-induced synchronization between chaotic units rely on the fact that the coupling should be active in the region where maximal transverse Lyapunov exponents are negative [45]. Besides, relative schemes for discontinuous interactions were proposed. The effect of a finite time step driving the response system to synchronization was analyzed [46]. In addition, the role of on–off coupling timescales in complex network synchronization has been explored [47]. It was found that the synchronization speed is accelerated when the on–off switching timescale is comparable to the timescale of the node dynamics. Relevant studies include synchronization of discrete and continuous systems using dynamic coupling [48] and emergent synchronization rhythms under dynamic interactions [49]. Moreover, an intermittent feedback has been proven to induce attractor selection [50] and steady states [51]. Motivated by these findings, a natural question is whether intermittent noise can promote complete synchronization in uncoupled chaotic systems? Therefore, we explore here the effect of Gaussian white noise injected only in a certain region of state space in uncoupled chaotic systems to achieve synchronization. Imparting the NIS, we devise a novel scheme that restricts the infusion of noise in particular state space. By restricting the noise in a certain region of state space, the growth of the attractor away from the *contraction region* is prevented which enables the trajectories to reside within the contraction region for a longer time. It is well established that the trajectories approaching the stable manifold of the saddle fixed point converges/contract thus diminishing the Lyapunov exponents to negative values. Hence, we design a scheme that allows the addition of noise to a restricted state space where optimal noise can be concentrated along the stable manifold of the saddle fixed point to achieve enhanced synchronization.

Remainder of the paper is organized as follows: in section 2, we describe general model of our approach and characterization methods. Numerical results are elucidated in section 3. We present the conclusive remarks in section 4.

2. The model

Let us consider two identical uncoupled chaotic systems driven by a common unbiased Gaussian white noise of the form,

$$\begin{aligned}\dot{\mathbf{X}}_1 &= F(X_1) + D\xi,\\ \dot{\mathbf{X}}_2 &= F(X_2) + D\xi,\end{aligned} \tag{1}$$

where, $\mathbf{X} \in \mathcal{R}^n$ is an n-dimensional vector describing the state variables of the model. The state variables are often denoted as $\mathbf{X} \in [x_1, x_2, \ldots x_n]^T$. $\mathbf{F}(\mathbf{X}) : \mathcal{R}^n \to \mathcal{R}^n$, is the nonlinear function that defines the chaotic evolution of the states. ξ denotes the white Gaussian noise having correlation $\langle \xi(t)\xi(t-\tau)\rangle = \delta(t)$ with the intensity D. It was shown that equation (1) exhibits synchronization for a particular strength of ξ [9]. To identify spatial constraints where the noise can be actively injected, equation (1) is rewritten as,

$$\begin{aligned}\dot{\mathbf{X}}_1 &= F(X_1) + D\alpha(\mathbf{X_1})\xi,\\ \dot{\mathbf{X}}_2 &= F(X_2) + D\ \alpha(\mathbf{X_2})\xi,\end{aligned} \tag{2}$$

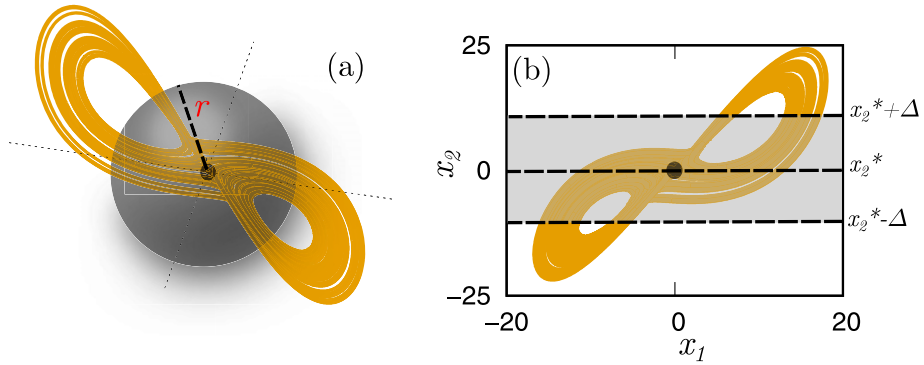

Figure 1. Schematic representation of the adopted strategy to choose the state-space region where noise can be added. The sphere with radius r with the center as origin determines the noise active region in state-space. (Lorenz attractor for illustrative purpose.) Here the normalized radius r shown in the figure is roughly $r \approx 0.5$. (b) Another scheme for regulating the noise by adding it to the trajectories by clipping along the x_2 variable in the state-space. Noise is active only in the region $x_2 \in (x_2^* - \Delta, x_2^* + \Delta)$ (gray region).

where, $\alpha(\mathbf{X})$ is defined as,

$$\alpha(\mathbf{X}) = \begin{cases} 1, & \text{if } (|\mathbf{X} - \mathbf{C}| \leqslant r'), \\ 0, & \text{if } (|\mathbf{X} - \mathbf{C}| > r'). \end{cases} \tag{3}$$

Here, $\mathbf{C}$ defines the center or unstable point of the attractor, usually the origin. The norm $|\mathbf{X} - \mathbf{C}|$ reflects the Euclidean distance of the state variables from the center. It should be noted that the noise perturbation depends on the state variables $\mathbf{X}$. The parameter r' which embodies the sphere of radius equal to $\sqrt{x_1^2 + x_2^2 + \cdots + x_n^2}$ designates the noise active region in the state-space. If $|\mathbf{X} - \mathbf{C}|$ falls within the radius r' the noise will be active in that region of state space and outside the sphere noise injection is absent. Precisely, the spatial constraint on the attractor where noise is applied depends on the magnitude of r'. For an illustration, we present a Lorenz attractor as shown in figure 1(a), i.e. $n = 3$. The sphere of radius r' with the center $\mathbf{C}$ as origin spans the region (gray sphere) in the attractor where noise can be added. We introduce the normalized parameter r as $r = r'/r_{\max}$, where $r_{\max}$ is the maximum radius of the attractor (in the absence of noise). Hence, $r \in [0, 1]$. As r increases, the region of the state space in which noise can be added increases proportionally. Another possibility for regulating the noise inflow into the trajectories is to choose one of the variables where noise has to be added, i.e. x_2 and applying the spatial constraint as, $\alpha(x_2) = 1$, when $x_2 \leqslant r$, otherwise 0. The scheme is illustrated in figure 1(b). The noise is added only when the desired variable lies within $r = x_2/x_2^{\max}$. Specifically, this model is effective when one starts to span the clipping region in the state space from x_2^* lying in the center. x_2^* denotes the unstable fixed point of the chosen system. Then the relevant subset of the attractor where noise is active is represented as $\mathcal{A}(r') = \{\mathbf{X} \in \mathcal{R}^n : |x_2 - x_2^*| \leqslant r'\}$. In addition, to impose a state-space constraint for the injection of noise, one can also adopt a two dimensional circular framework in a similar fashion along $x_1 - x_2$ or $x_2 - x_3$ plane. Irrespective of the schemes considered, we observe that the results presented here are qualitatively similar for the 1D and 2D state space constraints as well.

To ensure the occurrence of synchronization, we calculate the average synchronization error defined as the time average of the Euclidean distance between the two trajectories considered, $\langle E \rangle = \sqrt{(\mathbf{X}_1 - \mathbf{X}_2)^2}$. Then $\langle E \rangle \approx 0$ implies complete synchronization. For a quantitative understanding about the basin of the synchronized state in the phase space we calculate basin Stability ($S_{\mathcal{B}}$) [52], which is the normalized fraction of the volume of basin of attraction with respect to the synchronized state. It can be calculated as the ratio of the number of initial conditions that converge to the synchronized state to the total number of initial conditions. $S_{\mathcal{B}} = 1$ indicates that synchronization can be attained irrespective of the initial conditions. Further, we examine the maximum transverse Lyapunov Exponent ($\lambda_{\max}^{\perp}$) [2] in the transverse direction to the synchronization manifold. It is computed as $\lambda_{\max}^{\perp} = \lim_{t \to \infty} \frac{1}{t} \ln \frac{|\delta x(t)|}{|\delta x(0)|}$, where the small initial difference $\delta x(0) = x_1 - x_2$ evolves according to $\delta \dot{x} = \mathbb{D}f(x)\delta x$ along the transverse manifold. A necessary condition for synchronization is that $\lambda_{\max}^{\perp} < 0$. We also calculate the Shannon entropy $H(A)$ of the trajectories to quantify the synchronized state [53]. Also known as information entropy of an event A, H is a measure of the amount of information in a variable. For two simultaneous events A_1, A_2, which have m and n possibilities respectively, it can be calculated as $H(A_1, A_2) = -\sum_{i,j} P(i,j) \log P(i,j)$, where, $p(i,j)$ is the probability of the joint occurrence of i for A_1 and j for A_2. A sudden decrease in the joint entropy is an indication of the synchronization onset.

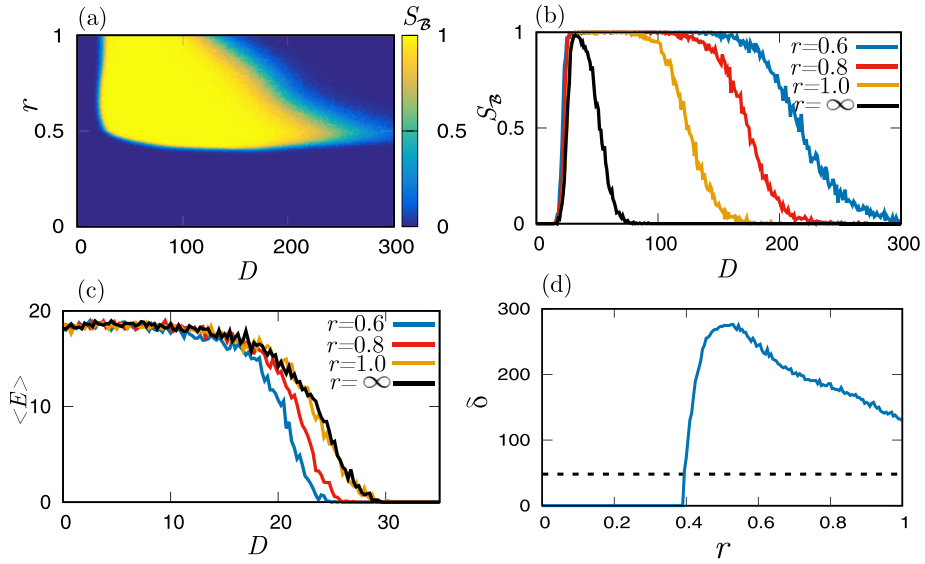

Figure 2. (a) The $D-r$ parameter space mapping the region of complete synchronization. The colorbar denotes the basin stability of SS ($S_{\mathcal{B}}$). (b) $S_{\mathcal{B}}$ for certain values of r including $r=\infty$ as a function of noise intensity D. (c) The average synchronization error $\langle E\rangle$ as a function of D. (d) The range of noise intensity δ where, synchronization persists as a function of r. The horizontal dotted line refers to the range of noise intensity for $r=\infty$ case.

3. Results

3.1. Lorenz oscillator

To begin with, we consider the classical Lorenz model to assimilate the approach. The model equations under considered framework are,

$$\begin{aligned}\dot{x}_1^i &= \sigma(x_2^i - x_1^i),\\ \dot{x}_2^i &= x_1^i(\rho - x_3^i) - x_2^i + D\alpha(x_1^i, x_2^i, x_3^i)\xi,\\ \dot{x}_3^i &= x_1^i x_2^i - \beta x_3^i,\end{aligned} \tag{4}$$

where, $i=1,2$ represent two independently evolving identical oscillators. The term $\alpha(.)\xi$ follows the same definition as equation (3). The parameters are chosen as $\sigma=10$, $\beta=8/3$ and $\rho=28$ such that equation (4) exhibit chaotic oscillations. The equations are integrated using the stochastic Euler method with the time step $\Delta t=0.001$. The perturbation in the form of additive intermittent noise along the x_2 direction allows the trajectories to enter into the *contraction* region. As a result, the $\mathrm{Re}(\Lambda_i)<0$ leads to complete synchronization Λ_i are the eigenvalues of the Jacobian matrices $J=\mathbb{D}f(x)$. $\alpha(.)$ restricts the injection of noise to a confined region of the state space, where the perturbation is effective to achieve synchronization. Consequently, the energy required for the task to be done is much less when compared to previous schemes, where the noise is added in the entire state space. In addition, the range of noise intensity that an attractor can accommodate without deformation is widely enhanced.

Figure 2(a) maps the region of complete synchronization in the $D-r$ plane. We consider 10^3 random initial conditions within the autonomous attractor range and plot the basin stability ($S_{\mathcal{B}}$) of the SS to obtain the phase diagram. The colorbar indicates the basin stability of SS. We can see that for $r<\approx 0.45$, there is no trace of synchronization regimes that signify the critical threshold of the restricted state space domain (r_c) above which the synchronization emerges. The SS persists only in the defined area in the $D-r$ plane which implies that beyond a certain level of noise intensity the synchronization breaks. However, at the onset of SS the critical noise intensity $D^C_{\min}$ remains roughly the same for all the values of r. Also, the range of D over which complete synchronization occurs, diminishes gradually with increasing r. For a clear picture, we plot the basin stability for selected values of r by varying D, figure 2(b). The range of noise intensity where SS appear with larger basin stability is found to increase with the decrease in r. It implies that the intermittent NIS endure for an extended range of noise intensity with enhanced $S_{\mathcal{B}}$. Here $r=\infty$ denote the addition of noise in the entire state space and $r=1$ stands for the actual size of an attractor. The intermittent common noise is added to two uncoupled chaotic systems in the limited state space with a constraint of $r<1$ for enhanced synchronization. Note that the attractor explores a larger state space with the addition of Gaussian noise. In the case of $r=\infty$, one can see that synchronization persists only for a

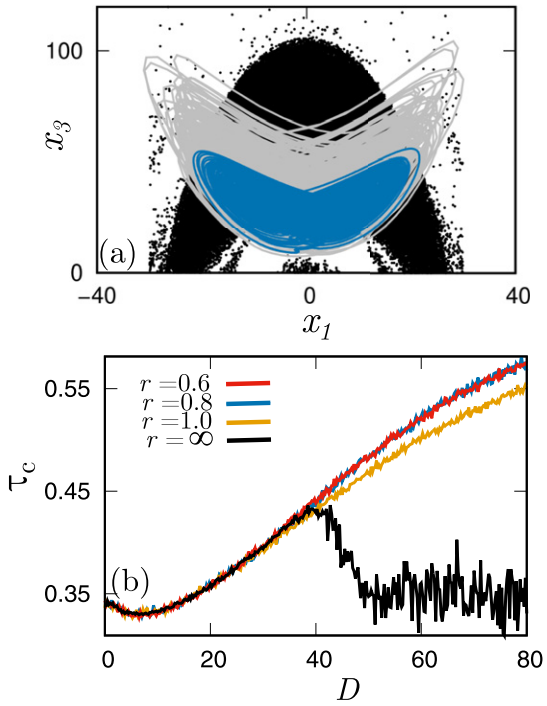

Figure 3. (a) The contraction region (black dots) in the plane $y = 0$ with the trajectories at $r = 0.6$ (blue) and $r = \infty$ (gray). (b) The average time spent by the trajectories in contraction region (τ_C) versus D at different r values.

shorter range of noise intensity and also the basin stability hardly reaches unity. This observation readily expresses the fact that our scheme aids the model to realize the SS with copious basin stability. In addition, the range of noise intensity where SS exists also hikes nearly threefold.

Further, we calculate the average synchronization error $\langle E \rangle$ with respect to D, figure 2(c). The $D^C_{\min}$ increases with the increase in r as inferred from the figure. To specify few cases, at $r = 0.6$ the $D^C_{\min} = 25$ and at $r = \infty$ the $D^C_{\min} = 29$. This illustrates the advantage of the considered scheme over the previous strategies. Dynamically, the intermittent noise allows the trajectories to comprehend more perturbations in the contraction region and thus trapping them there for a long time. Also, it induces a contraction of nearby trajectories at the neighborhood of the unstable manifold rather than expansion that additionally assists the SS. For further exploration, we measure the range of noise intensity where synchronization persists in the model as $\delta = D^C_{\max} - D^C_{\min}$. Taking into account that the SS vanishes after certain noise intensity, the study of δ is inevitable. We find that for $0.4 \leqslant r \leqslant 0.55$, δ increases sharply and starts to decline after the mark. The dotted black line in the figure denotes the $\delta \approx 48$ at $r = \infty$, figure 2(d). This property ensures the advantage of adding intermittent noise according to spatial constraint. We also see the marked difference in δ between $r = \infty$ and other values of r.

To conceive the mechanism, we plot the contraction region on the $x - z$ plane along with the trajectories at two different values of r as shown in figure 3(a). The contraction region is calculated from the $\mathbb{D}f(x)$ and whenever the $\mathrm{Re}(\Lambda_i) < 0$ the coordinates are marked to represent the region. One can readily see that the trajectory at $r = 0.6$ (blue) resides well within the contraction region. In contrast, at $r = \infty$ (gray), due to larger and continuous noise injection in the entire state space, the trajectories are out of bound from the contraction region. This may cause a synchronization loss at larger noise intensities. Nevertheless, by introducing the intermittent noise based on the spatial constraint, one can confine the trajectories within the contraction region. To get an insight, we have computed the average time spent by the trajectories in the contraction region (τ_C) for D, figure 3(b). As we see from the figure 3(b), even for larger D, the τ_C increases for the lesser values of r. For instance, at $r = 0.6$, the $\tau_C > 0.5$ which is very crucial to achieve synchronization at larger noise intensities. Conversely, at $r = \infty$, the τ_c is substantially reduced which deters complete synchronization. Due to the limitation of noise in particular state space, the consolidated noise injected into the trajectories is consistently lesser than the applied noise. This allows the trajectories to dwell in the contraction region for a longer interval of time even at larger D.

To concur the observed synchronization, in figure 4(a), we present the $\lambda^{\perp}_{\max}$ at different values of r. From the figure, we see that the $\lambda^{\perp}_{\max}$ becomes negative at respective $D^C_{\min}$. This property denotes the stabilization of the transverse manifold after $D^C_{\min}$ beckoning the onset of synchronization. The $D^C_{\min}$ recorded at $r = 0.6$, matches fairly well with the transition point incurred from $\langle E \rangle$. Further, we examined

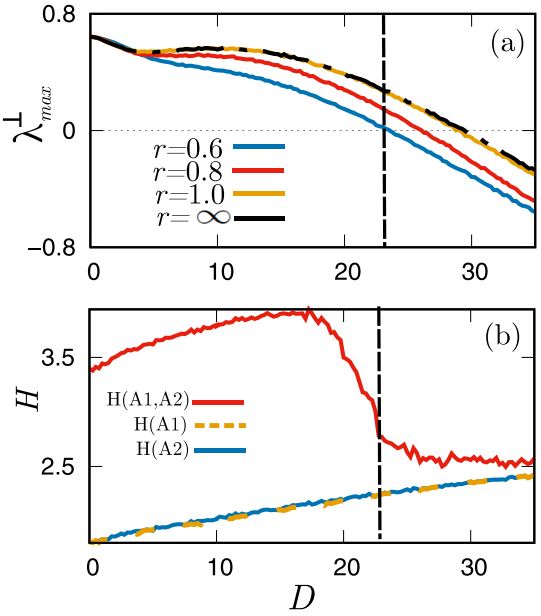

Figure 4. (a) Maximal transverse Lyapunov exponent ($\lambda^{\perp}_{\max}$) versus D. (b) Shannon entropy of the individual and combined system as a function of D. The dotted line indicate the $D^{C}_{\min}$ at the onset of synchronization.

the Shannon entropy at $r = 0.6$ to point out the onset of synchronization. Figure 4(b) shows the $H(A_{1(2)})$ for the individual (dotted lines) and $H(A_1, A_2)$ for the combined attractors (red). The entropy of the combined attractors suffers a sudden drop at the $D^{C}_{\min}$ indicating the synchronization onset. However, the entropy of the individual attractors invariably increased following the universal principle.

3.2. PR circuit model

Next, we consider a realistic circuit model namely, the Pikovski–Rabinovich (PR) circuit where one can find feasible chances of realizing the results through experiments. The PR circuit model is given by the following equations:

$$\begin{aligned}
\dot{x}^i_1 &= x^i_2 - \beta x^i_3,\\
\dot{x}^i_2 &= -x^i_1 + 2\gamma x^i_2 + \rho x^i_3,\\
\dot{x}^i_3 &= [x^i_1 - (x^i_3)^3 + x^i_3]/\mu + D\alpha(x^i_1, x^i_2, x^i_3)\xi,
\end{aligned} \tag{5}$$

with $\beta = 0.66$, $\rho = 0.165$, $\gamma = 0.201$ and $\mu = 0.047$. Here, $i = 1, 2$ indicate two individual oscillators without coupling. Equation (5) is a normalized equation of the nonlinear oscillator with a negative resistance and a tunnel diode [54]. The noise has been added in the x_3 direction to stabilize the cubic nonlinearity $F(x_3) = x^3_3 + x_3$ corresponding to the tunnel diode in the circuit. Note that the $\alpha(.)\xi$ regulates the noise infusion following equation (3).

Figure 5(a) shows the $D - r$ parameter space calculated based on the $S_{\mathcal{B}}$. Below $r = 0.4$, the additive noise fails to bring synchrony in the oscillators irrespective of the noise intensity. When $r > 0.45$, there is an onset of complete synchronization for values of $D > D^{\min}_{C}$. After a certain interval of $D^{\min}_{C} \geqslant D \leqslant D^{\max}_{C}$ the synchronization vanishes due to destabilization of the synchronization manifold. To verify the enhancement of basin stability, we plot $S_{\mathcal{B}}$ versus D for various radii of noise injection. As seen from the figure the $S_{\mathcal{B}}$ and δ are significantly high in the range $0.6 \geqslant r \leqslant 0.8$. In particular, we find that $r = 0.6$ will be the most optimum radius of noise injection in this model to achieve CS. Besides, we calculate $\langle \mathrm{E} \rangle$ with respect to D for various r. It is clearly evident that for smaller r, lets say, $r = 0.4$, the onset of synchronization occurs at $D \approx 3.5$ from figure 5(c). Upon increasing r, one may notice the emergence of synchronization at lesser D. As a special case, at $r = 0.6$ the synchronization takes place at $D = 2.64$ while for $r = \infty$, $D = 2.66$. In figure 5(d), we show the variation of δ with r. We see that in the interval $0.4 \geqslant r \leqslant 0.8$ the range of noise intensity where synchronization is observed has been significantly enhanced when compared to $r = \infty$ (horizontal dotted line).

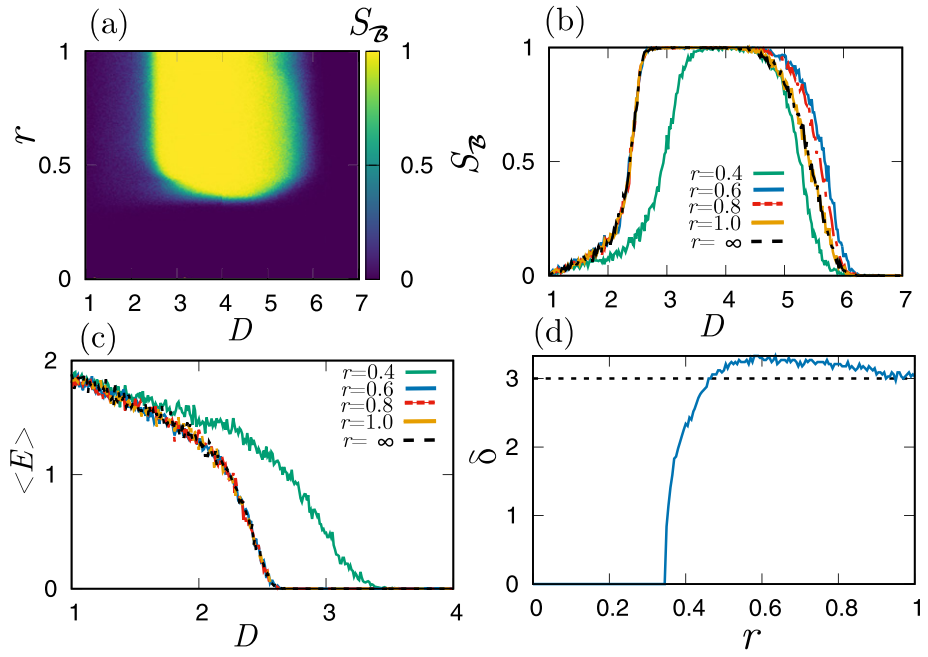

Figure 5. Analysis of the model equation (5). (a) The $D-r$ parameter space mapping the region of complete synchronization. The colorbar denotes the basin stability of SS (S_B). (b) S_B for certain values of r including $r=\infty$ as a function of the noise intensity D. (c) The average synchronization error $\langle E\rangle$ as a function of D. (d) The range of noise intensity δ where, synchronization persists as a function of r. The horizontal dotted line refers to the range of noise intensity for $r=\infty$.

3.3. HR neuron model

To verify the universality of the approach, we study the Hindmarsh–Rose (HR) [55] neuron model. It exhibits alternating quiescence and excited oscillations mimicking the dynamics of the neurons. The equations under the considered framework is as follows,

$$\begin{aligned}\dot{x}_1^i &= x_2^i - a(x_1^i)^3 + b(x_1^i)^2 - x_3^i + I + D\alpha(x_1^i)\xi,\\ \dot{x}_2^i &= c - d(x_1^i)^2 - x_2^i,\\ \dot{x}_3^i &= \rho[S(x_1^i - \chi) - x_3^i],\end{aligned} \tag{6}$$

with $a=1$, $b=3$, $c=1$, $d=5$, $S=4$, $\rho=0.006$, $\chi=-1.56$ and $I=3$. Here, $i=1,2$ denotes two self oscillating neurons. The condition $\alpha(.)\xi$ is modified as,

$$\alpha(x_1) = \begin{cases} 1, & \text{if } (x_1 \leqslant r'),\\ 0, & \text{if } (x_1 > r'). \end{cases} \tag{7}$$

Note that the regulating condition for the noise infusion is restricted to the x_1 variable. We have checked the applicability of equation (3) in the HR model but found trivial results due to the drastic difference in the dynamics.

Figure 6(a) maps the $D-r$ parameter space where complete synchronization appears in equation (6). One can notice that the onset of synchronization appears beyond $r\approx 0.4$ at critical D_C. The $D_C^{\min}$ remains unchanged for all values of r. Also, we found that as r increases the synchronization region shrinks with the increase in D. This may be due to the larger noise intensity and the area of injection leading to an instability of the synchronization manifold. We also notice that the attractor smears out with the addition of noise. The basin stability as a function of D at different values of r is shown in figure 6(b). In this model, we do not find a significant improvement in the basin stability as a function of r. However, with the increase in D the S_B suffers minor dips and shows a gradual decline until $D_C^{\max}$. We find that $r=0.6$ enables sustained S_B and a larger range of noise intensity for SS. We capture the synchronization onset by calculating $\langle E\rangle$ with D for certain values of r. The $D_C^{\min}$ remains unchanged at all values of r. The null value of $\langle E\rangle$ indicate the complete synchronization as shown in figure 6(c). Further, we plot the variation in δ with r to record the advantage of the scheme, figure 6(d). We find that only in a smaller interval $0.5\geqslant r\leqslant 0.65$ there exists an enlarged range of noise intensity where synchronization persist. For the rest of the r values the δ remains approximately close to $\delta\approx 20$.

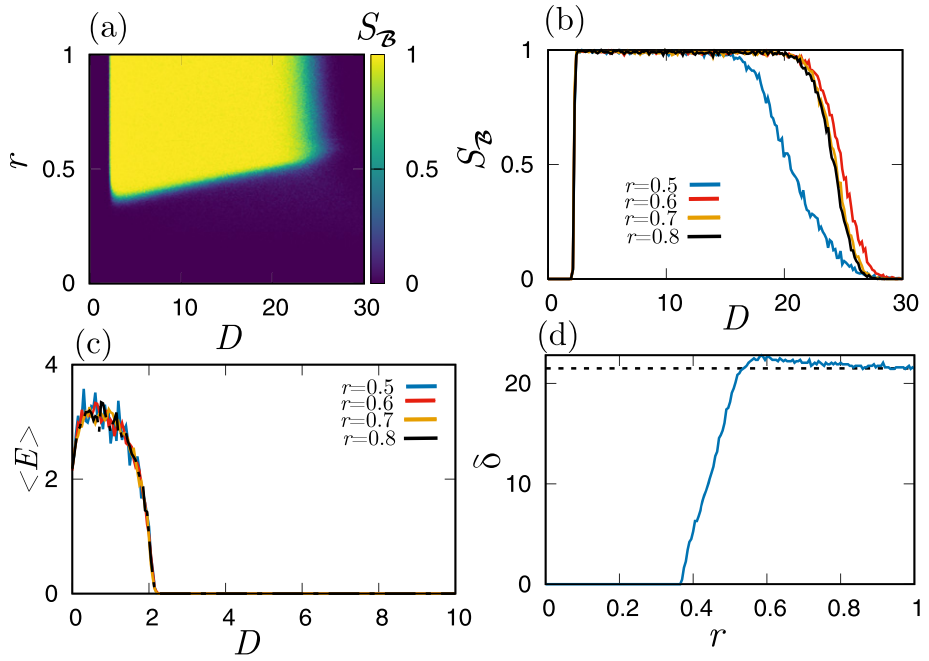

Figure 6. Analysis of model equation (6). (a) The $D - r$ parameter space mapping the region of complete synchronization. The colorbar denotes the basin stability of SS (S_B). (b) S_B for certain values of r as a function of the noise intensity D. (c) The average synchronization error $\langle E \rangle$ as a function of D. (d) The range of noise intensity δ where, synchronization persists as a function of r. The horizontal dotted line refers to the range of noise intensity for $r = \infty$.

4. Conclusion

In summary, we explored the effect of state-space dependent intermittent noise that is being injected into the trajectories of a chaotic system. We found that intermittent noise enhances the complete synchronization among uncoupled chaotic units. The mechanism beneath the synchronization attributes to the constrained noise in the state-space that regulates the chaotic trajectories to asymptotically evolve within the contraction region. As a consequence, the real part of the Jacobian $\mathbb{D}f(x)$ possesses negative eigenvalues that signify synchronization state. Moreover, the scheme ensures a wider range of noise intensity where the SS persist. It is important to note that the restricted noise amplifies the basin stability of the synchronization state. This may be due to the localized noise perturbation suffered by the trajectories leading to the convergence of a larger set of initial conditions toward SS. These findings were concurred by the numerical outcomes of the Lorenz system, PR chaotic circuit and HR neuron model. The condition for regulating noise infusion in chaotic systems holds $\alpha(\mathbf{X})$ while for excitable model it is a function of one variable $\alpha(x_1)$. The intermittent noise is also effective in inducing synchronization in a network of uncoupled chaotic oscillators. We believe that the optimizing region of active noise for enhancing synchronization may have potential applications to lasers, electronic circuits, neuronal and communication systems etc. In addition, an interesting work will be to verify the results and the robustness of the scheme through experiments.

Acknowledgments

ES thanks University Grants Commission (UGC), India for supporting through a fellowship. MDS, MPA and SD acknowledges financial support from the Department of Science and Technology (DST), India (Grant Nos. EMR/2016/005561 and INT/RUS/RSF/P-18). JK was supported by the Russian Ministry of Education and Science (Agreement No. 075-15-2020-808).

Data availability statement

All data that support the findings of this study are included within the article (and any supplementary files).

ORCID iDs

Manish Dev Shrimali https://orcid.org/0000-0003-1633-469X

References

[1] Boccaletti S, Kurths J, Osipov G, Valladares D L and Zhou C S 2002 *Phys. Rep.* **366** 1–101
[2] Pikovsky A, Rosenblum M and Kurths J 2001 *Synchronization: A Universal Concept in Nonlinear Sciences* (Cambridge: Cambridge University Press)
[3] Balanov A, Janson N, Postnov D and Sosnovtseva O 2008 *Synchronization: From Simple to Complex* (Berlin: Springer)
[4] Ho M-C and Hung Y-C 2002 *Phys. Lett.* A **301** 424–8
[5] Huang L, Feng R and Wang M 2004 *Phys. Lett.* A **320** 271–5
[6] Chen H 2005 *Chaos Solitons Fractals* **23** 1245–51
[7] Han X, Lu J-A and Wu X 2004 *Chaos Solitons Fractals* **22** 221–7
[8] Tan X, Zhang J and Yang Y 2003 *Chaos Solitons Fractals* **16** 37–45
[9] Zhou C and Kurths J 2002 *Phys. Rev. lett.* **88** 230602
[10] Zaks M A, Park E-H and Kurths J 2000 *Int. J. Bifurcation Chaos* **10** 2649–67
[11] Matsumoto K and Tsuda I 1983 *J. Stat. Phys.* **31** 87–106
[12] Yoshimoto M, Shirahama H and Kurosawa S 2008 *J. Chem. Phys.* **129** 014508
[13] Sánchez E, Matias M A and Perez-Munuzuri V 1997 *Phys. Rev.* E **56** 4068
[14] Neiman A B and Russell D F 2002 *Phys. Rev. Lett.* **88** 138103
[15] Toral R, Mirasso C R, Hernández-Garcıa E and Piro O 2001 *Chaos* **11** 665–73
[16] Nakao H, Arai K and Kawamura Y 2007 *Phys. Rev. Lett.* **98** 184101
[17] Nagai K H and Kori H 2010 *Phys. Rev.* E **81** 065202
[18] Russo G and Shorten R 2018 *Physica* D **369** 47–54
[19] Grenfell B T, Wilson K, Finkenstädt B F, Coulson T N, Murray S, Albon S D, Pemberton J M, Clutton-Brock T H and Crawley M J 1998 *Nature* **394** 674–7
[20] Mainen Z F and Sejnowski T J 1995 *Science* **268** 1503–6
[21] Vaidya J, Bashar M K and Shukla N 2021 *Sci. Rep.* **11** 1–8
[22] Touboul J D, Piette C, Venance L and Ermentrout G B 2020 *Phys. Rev.* X **10** 011073
[23] Zambrano S, Mariño I P, Seoane J M, Sanjuán M A F, Euzzor S, Geltrude A, Meucci R and Arecchi F T 2010 *New J. Phys.* **12** 053040
[24] Liao Z, Ma K, Tang S, Sarker M S, Yamahara H and Tabata H 2021 *Chaos Solitons Fractals* **151** 111262
[25] Gómez-Gardeñes J, Gómez S, Arenas A and Moreno Y 2011 *Phys. Rev. Lett.* **106** 128701
[26] Zhang X, Boccaletti S, Guan S and Liu Z 2015 *Phys. Rev. Lett.* **114** 038701
[27] Zhang X, Hu X, Kurths J and Liu Z 2013 *Phys. Rev.* E **88** 010802
[28] Boccaletti S, Almendral J A, Guan S, Leyva I, Liu Z, Sendiña-Nadal I, Wang Z and Zou Y 2016 *Phys. Rep.* **660** 1–94
[29] Arenas A, Díaz-Guilera A, Kurths J, Moreno Y and Zhou C 2008 *Phys. Rep.* **469** 93–153
[30] Li X *et al* 2020 *New J. Phys.* **22** 123026
[31] Dai X, Li X, Gutiérrez R, Guo H, Jia D, Perc M, Manshour P, Wang Z and Boccaletti S 2020 *Chaos Solitons Fractals* **132** 109589
[32] Dai X, Li X, Guo H, Jia D, Perc M, Manshour P, Wang Z and Boccaletti S 2020 *Phys. Rev. Lett.* **125** 194101
[33] Zhuang J, Cao J, Tang L, Xia Y and Perc M 2020 *IEEE Trans. Syst. Man Cybern Syst.* **50** 4807–16
[34] Panahi S, Nazarimehr F, Jafari S, Sprott J C, Perc M and Repnik R 2021 *Appl. Math. Comput.* **394** 125830
[35] Hussain I, Jafari S, Ghosh D and Perc M 2021 *Nonlinear Dyn.* **104** 2711–21
[36] Shafiei M, Jafari S, Parastesh F, Ozer M, Kapitaniak T and Perc M 2020 *Commun. Nonlinear Sci. Numer. Simul.* **84** 105175
[37] Wang Q, Chen G and Perc M 2011 *PLoS one* **6** e15851
[38] Parastesh F, Azarnoush H, Jafari S, Hatef B, Perc M and Repnik R 2019 *Appl. Math. Comput.* **350** 217–23
[39] Wang Q, Perc M, Duan Z and Chen G 2009 *Phys. Rev.* E **80** 026206
[40] Faghani Z, Wang Z, Parastesh F, Jafari S and Perc M 2020 *Int. J. Bifurcation Chaos* **30** 2050123
[41] Nazarimehr F, Panahi S, Jalili M, Perc M, Jafari S and Ferčec B 2020 *Appl. Math. Comput.* **372** 124996
[42] Chowdhury S N, Majhi S, Ozer M, Ghosh D and Perc M 2019 *New J. Phys.* **21** 073048
[43] Schröder M, Mannattil M, Dutta D, Chakraborty S and Timme M 2015 *Phys. Rev. Lett.* **115** 054101
[44] Tandon A, Schröder M, Mannattil M, Timme M and Chakraborty S 2016 *Chaos* **26** 094817
[45] Ghosh A, Godara P and Chakraborty S 2018 *Chaos* **28** 053112
[46] Amritkar R E and Gupte N 1993 *Phys. Rev.* E **47** 3889
[47] Chen L, Qiu C and Huang H B 2009 *Phys. Rev.* E **79** 045101
[48] Junge L and Parlitz U 2001 *Phys. Rev.* E **64** 055204
[49] Dixit S, Nag Chowdhury S, Prasad A, Ghosh D and Shrimali M D 2021 *Chaos* **31** 011105
[50] Yadav K, Kamal N K and Shrimali M D 2017 *Phys. Rev.* E **95** 042215
[51] Dixit S, Sharma A, Prasad A and Shrimali M D 2019 *Int. J. Dynam. Control* **7** 1015–20
[52] Menck P J, Heitzig J, Marwan N and Kurths J 2013 *Nat. Phys.* **9** 89–92
[53] Shannon C E 1948 *Bell Syst. Tech. J.* **27** 379–423
[54] Pikovskii A S and Rabinovich M I 1978 *Dokl. Akad. Nauk SSSR* **239** 301–4
[55] Hindmarsh J L and Rose R M 1984 *Proc. R. Soc.* B **221** 87–102